Available online at www.sciencedirect.com
SCIENCE DIRECT®
Journal of Computational Physics 202 (2005) 463–487
JOURNAL OF COMPUTATIONAL PHYSICS
www.elsevier.com/locate/jcp

Precise computations of chemotactic collapse using moving mesh methods

C.J. Budd [a], R. Carretero-González [b,*], R.D. Russell [c]

[a] Department of Mathematical Sciences, University of Bath, Claverton Down, Bath BA2 7AY, UK
[b] Nonlinear Dynamical Systems Group, Department of Mathematics and Statistics, San Diego State University, San Diego, CA 92182-7720, USA
[c] Department of Mathematics and Statistics, Simon Fraser University, Burnaby, BC, Canada V5A 1S6

Received 3 October 2003; received in revised form 15 April 2004; accepted 23 July 2004
Available online 11 September 2004

Abstract

We consider the problem of computing blow-up solutions of chemotaxis systems, or the so-called chemotactic collapse. In two spatial dimensions, such solutions can have approximate self-similar behaviour, which can be very challenging to verify in numerical simulations [cf. Betterton and Brenner, Collapsing bacterial cylinders, Phys. Rev. E 64 (2001) 061904]. We analyse a dynamic (scale-invariant) remeshing method which performs spatial mesh movement based upon equidistribution. Using a suitably chosen monitor function, the numerical solution resolves the fine detail in the asymptotic solution structure, such that the computations are seen to be fully consistent with the asymptotic description of the collapse phenomenon given by Herrero and Velázquez [Singularity patterns in a chemotaxis model, Math. Ann. 306 (1996) 583–623]. We believe that the methods we construct are ideally suited to a large number of problems in mathematical biology for which collapse phenomena are expected.

PACS: 87.17.Jj; 87.18.Bb; 87.18.Ed; 02.60.Cb
Keywords: Chemotaxis; Blow-up; Collapse; Adaptive mesh methods

1. Introduction

There is currently considerable interest in the modelling and numerical solution of systems of reaction diffusion problems arising in many applications areas of the physical sciences. One important class, repre-

* Corresponding author. Tel.: +1 619 594 7252; fax: +1 619 594 2029.
E-mail addresses: cjb@maths.bath.ac.uk (C.J. Budd), rdr@cs.sfu.ca (R.D. Russell).
URLs: http://nlds.sdsu.edu, http://www.rohan.sdsu.edu/~rcarrete.

0021-9991/$ - see front matter © 2004 Elsevier Inc. All rights reserved.
doi:10.1016/j.jcp.2004.07.010

sentative of the complexities which can arise, involve problems in mathematical biology where living systems respond to external stimuli. There are various basic types of such responses, described using the suffix *t*-axis (Greek for ''arrange, turning''). A typical one, and the one studied in this paper, is a *chemotaxis* problem [3–5] where the *t*-axis is triggered by chemical gradients.

The resulting mathematical models are typically nonlinear systems of reaction diffusion partial differential equations (PDEs) which pose a number of analytical and computational challenges. First, analysis is complicated by the fact that it is a system of PDEs. There is often only a formal analysis or prediction of solution behaviour, and one wishes to approximate the solution numerically to confirm theoretical results. Second, the solution behaviour itself can be complicated. A particular feature of this is a blow-up in one or more solution components in a finite time T, generally referred to as a *collapse*, which occurs over a diminishing length scale. Collapse is observed in the chemotaxis problem as well as in many other physical systems such as the closely related problem of gravitational collapse studied in [6–9].

Collapse-type phenomena are nontrivial to compute under the best of conditions, and a very careful numerical approach is required to correctly resolve the fine structure of the behaviour and to avoid misleading answers. For the physical situations of interest, the solution can be particularly complex, with subtle scaling relationships between time and space leading to only approximately self-similar structure.

Exact blow-up solutions in one spatial dimension (1D) were studied by Levine and Sleeman [10] for a class of chemotaxis equations without chemical diffusion and without chemical decay. They showed the blow-up profile to be self-similar, with the cell concentration tending to a Dirac-delta with ''height'' inversely proportional to the time to blow-up.

The general chemotaxis system is a problem with surprisingly delicate behaviour in two spatial dimensions (2D). Its solutions can exhibit local collapse for which the behaviour is believed to be *not* strictly self-similar, i.e., it does not obey the underlying scaling laws of the PDE. Moreover, the structure away from the blow-up point is complicated, with blow-up in time and space not following a strict power law, but obeying an approximate power law with a logarithmic correction. An asymptotic description of this behaviour is given in [2], and it is shown in [11] that this blow-up mechanism is stable. However, in [2,11] there is no proof of the uniqueness of this blow-up behaviour, and in [1] some numerical evidence is presented which indicates that other types of blow-up might be possible. In three spatial dimensions (3D) the situation is much clearer, with the collapse occurring in a self-similar manner, obeying a strict power law, and numerical verification of this solution behaviour fairly straightforward to perform.

Capturing the solution behaviour precisely is a particularly challenging numerical problem in 2D, as exemplified by the numerical results (based on a static regridding approach) presented in [1] which had some anomalies that left some unresolved issues, suggesting to the authors of this paper that further research into the numerical approximation is needed. This forms the background for our paper. We shall use a high order moving mesh method to obtain a careful resolution of the collapse behaviour. The results give support to the conjecture that the asymptotic behaviour derived in [2] is unique and globally attracting.

Our approach is a development of the one described in [12] in which a semi-discrete dynamic regridding method is used together with a high order (in both space and time) resolution of the solution. Central to this procedure is the allocation of the mesh points through the solution of so-called moving mesh PDEs, or MMPDEs [13]. This is done by equidistributing a monitor function chosen in such a manner that any scaling laws which are present in the solution should be inherited in the numerical method, but these scaling laws are *not* imposed a-priori on the method. (The danger of the latter is that it can potentially lead to misleading observations of self-similar behaviour which may not be present in the underlying problem).

For problems with true self-similar blow-up, there is a region close to the origin in which all of the blow-up occurs in a similar manner, and the solution matches smoothly onto an exterior region. For such problems general adaptive numerical methods based upon the use of MMPDEs are developed in [14,15], and a general theory describing their performance is possible [16]. But for the non-self-similar case treated here, it is a much more delicate task to assure that the proper solution behaviour is computed. Whilst the broad

outline of the methods described in [12] is still applicable, the choice of the correct monitor function leads to a delicate play-off between the requirements of using a fine enough mesh to resolve the solution and avoiding stiffness in solving the resulting system of ordinary differential equations (ODEs). However the results obtained with this method compare very well with the asymptotic results of [2], giving us confidence in using the MMPDE based approach for a wider range of collapse problems.

The outline of the paper is as follows. In Section 2, we describe the chemotaxis system and outline the asymptotic theory of Herrero and Velázquez [2]. In Section 3, we outline the numerical method and give the results of the numerical computations. These lend strong support to the correctness of the asymptotic theory in [2] which we examine through a careful series of comparisons. In Section 4, we provide more analysis of the numerical method, in particular showing how the monitor function determining the mesh is derived. Section 5 contains some more detailed numerical results related to the mesh motion. Finally, in Section 6, we draw some conclusions and indicate how our approach could be used for other collapse problems.

2. The chemotaxis system

2.1. The equations

The non-dimensional chemotaxis equations have the form

$$\begin{cases} u_t = \nabla^2 u - \chi \nabla \cdot (u \nabla v), \\ v_t = \nabla^2 v + u - v, \end{cases} \tag{1}$$

where we take $\mathbf{r} \in \Omega = \{\mathbf{r}:|\mathbf{r}| \leqslant R\}$, $\chi = 8$ for convenience (see [2]), and enforce Neumann boundary conditions for u and v on $\partial\Omega$. This model represents the evolution of a cell density $u(\mathbf{r},t)$, in the presence of a chemical substrate $v(\mathbf{r},t)$ [4,5,17]. The substrate, or chemo-attractant, is produced by the cells and in turn attracts cells via the cross diffusion term with chemotactic coefficient χ. In this process, the total mass of the cell population given by

$$\int_\Omega u \, \mathrm{d}\mathbf{r} \tag{2}$$

is constant throughout the evolution.

The overall effect of the cross diffusion term is to create cell aggregates that may collapse in a finite time T so that both u and v become unbounded in this limit. Collapse is generally radially symmetric, at least locally, so without loss of generality we assume that the solutions u and v are radially symmetric and become unbounded at the origin $r = 0$.

Some authors [18–25] consider the related problem of taking $v_t = 0$ [25]. It is not clear to us when the solution to this simpler problem can be used to provide a solution to the general problem (1), although this term can be shown to be formally small in a certain asymptotic limit [18,24]. It is certainly true that v evolves much more slowly than u. The strength of the numerical approach we describe is that in principle it can solve any number of coupled physical PDEs in their general form.

Our investigation will be mainly concentrated on the case where the dimension of the space Ω is $d = 2$, for which the blow-up is not strictly self-similar. For $d = 3$, there is also a set of blow-up profiles (concentrated at the origin) which are strictly self-similar and obey a simple power law [23]. We also compute the solution for this simpler case using the techniques in [12]. Any such self-similar solution corresponds to a rescaled function which is constant in rescaled time. The solution behaviour for $d = 2$ is much more subtle,

and must be determined in this case by using centre-manifold type arguments [2]. For the remainder of the paper we consider the case $d = 2$ unless stated otherwise.

2.2. A description of the blow-up solution

The asymptotic form of the solution of (1) has been analysed in some detail by Herrero and Velázquez [2,11]. In particular, a structure for the blow-up profile is proposed which is shown to be locally stable. No uniqueness (or global stability) is established. While an alternative asymptotic form for the collapse has been proposed in [1], our numerical computations are strongly supportive of the results given by [2], and hence we restrict our discussion to this latter form. As is usual with most descriptions of blow-up phenomena where $u(0,t) \to \infty$ as $t \to T$, we see two different descriptions of the form of the solution, an *inner* or *core* region where it evolves rapidly in both time and space, and an *outer* region where it evolves to a (singular) limiting profile. A successful numerical method must capture both forms of behaviour.

At the blow-up time $t = T$, $u(r,t)$ takes the limiting form

$$u(r, T) = \pi\delta(r) + \psi(r), \tag{3}$$

where $r = |\mathbf{x}|$, δ is the $\mathbb{R}^2$ delta function, and $\psi(r)$ is a *singular* function at $r = 0$ [2]. It is important to mention that the limiting form (3) is only valid near the blow-up region (where boundary effects can be neglected).

Crucial to the subsequent analysis are the facts that (*i*) $\psi(r)$ is *integrable* in $\mathbb{R}^2$ and (*ii*) $\psi(r)^{1/2}$ is integrable in $\mathbb{R}^1$. Observe that $u(0,T) = \infty$.

The time variation of $u(0,t)$ close to the blow-up time is complicated when $d = 2$. The asymptotic structure of a particular form of this solution was studied by Herrero and Velázquez [2,11]. For their singular solution, in the limit of $(T - t) \to 0$,

$$\gamma \equiv u(0, t) = L^{-2}\left(1 + \mathcal{O}\left(\frac{\log(\tau)}{\sqrt{\tau}}\right)\right), \tag{4}$$

where

$$\tau = -\log(T - t).$$

In this expression, $L(t)$ is a natural length scale for the problem given by

$$L(t) = K(T - t)^{1/2}\, \mathrm{e}^{-|\log(T-t)|^{1/2}/\sqrt{2}}\left(1 + \mathcal{O}\left(\frac{\log(\tau)}{\sqrt{\tau}}\right)\right) = K(T - t)^{0.5+\alpha}\left(1 + \mathcal{O}\left(\frac{\log(\tau)}{\sqrt{\tau}}\right)\right), \tag{5}$$

where

$$\alpha = 1/\sqrt{2\,|\log(T - t)\,|} \tag{6}$$

and K is a constant.

The most significant feature of this description of blow-up is that $u(0,t)$ and $L(t)$ do not obey an asymptotic power law. However, testing this conclusion is difficult numerically because of the slow convergence of the asymptotic series. In particular, the error term is proportional to $\log(\tau)/\sqrt{\tau}$. As $\tau = -\log(T - t)$, $1/\sqrt{\tau}$ is proportional to $1/\sqrt{\log(u(0,t))}$, so for this to be small, we must take $u(0,t)$ to be very large. This is precisely the challenge faced when doing such computations and which we address in this paper. In particular, we are able to compute solutions for which $u(0,t) \approx 10^{20}$ so that $1/\sqrt{\log(u(0,t))} \approx 0.14$. Whilst not as small as we would like, this error bound is small enough that the computational results, and in particular the

agreement between the numerically computed values and the leading order asymptotic formulae, indicate that the asymptotic results are sharp.

In the case of true self-similar blow-up (where the solution is invariant under the scaling laws which apply to the differential equation) we expect to see the simpler power law relation

$$u(0,t) \sim (T-t)^{-1}, \quad L(t) \sim (T-t)^{0.5}.$$

Only if we formally set $\alpha = 0$ into the formula (5) do we see this form of behaviour. We do observe such self-similar behaviour in the evolution of the solutions of the chemotaxis equations in *three dimensions*. Limiting power law behaviour is also observed in the computations described in [1].

2.2.1. The core region

Herrero and Velázquez [2,11] analyse the spatial structure close to blow-up by looking at the centre-manifold of the solution expressed in a set of rescaled coordinates derived from the canonical symmetry reduction of the original equation. By doing this they obtain rigorous results concerning the limiting behaviour of a class of blow-up solutions. In particular, it is shown in these papers that in the *core region* close to the blow-up point at the origin the function $u(r,t)$ takes the form

$$u(r,t) = \gamma \bar{u}(\gamma^{1/2} r) \equiv \frac{\gamma}{(1+\gamma r^2)^2}\left(1 + \mathcal{O}\left(\frac{\log(\tau)}{\sqrt{\tau}}\right)\right), \tag{7}$$

where as before $\gamma = u(0,t)$. The form of $u(r,t)$ is illustrated in Fig. 1. The convergence to this asymptotic profile is also shown in these papers to be uniform on sets $|r| \leqslant L(t)$ given in (5). (In this context, where functions develop singularities in finite time, uniform convergence implies that the scaled solution $L(t)^2 u(r,t)$ converges to the scaled asymptotic solution along level curves of the scaled variable $y = r/L(t)$.)

Furthermore, the mass of u in the core is constant with

$$\int_{\mathbb{R}^2} \bar{u}\, \mathrm{d}\mathbf{x} = 2\pi \int_0^\infty \bar{u}(r,t) r\, \mathrm{d}r = \pi.$$

In the sense of distributions, $\bar{u}(r,T) = \pi\delta(r)$ (cf. (3)). Both $\bar{u}$ and $\sqrt{\bar{u}}$ are integrable over the real line $\mathbb{R}$, with the integral of $\bar{u}$ proportional to $\gamma^{1/2}$ and the integral of $\sqrt{\bar{u}}$ independent of γ.

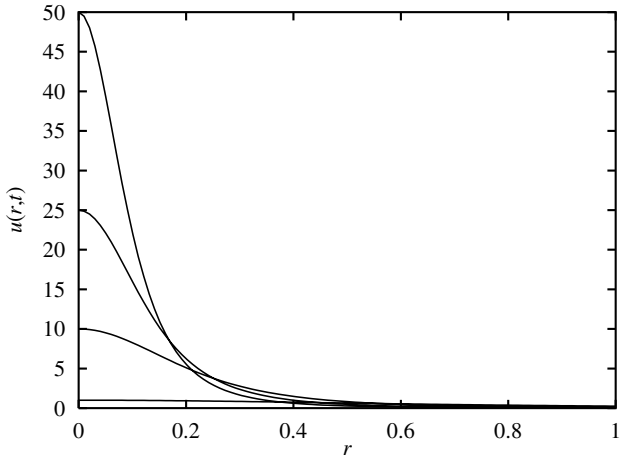

Fig. 1. The behaviour of u in the core region for varying γ.

Here, the dependence of the core width $L(t)$ on the blow-up time $(T-t)$ does not follow a simple exponential law. The corrections to this exponential relation break the self-similarity, complicating any effort to use self-similar blow-up numerical techniques [12].

Note that the time dependence of the core region solution (7) enters via the term $\gamma = \gamma(t)$, viz., the natural length scale

$$L(t) = \frac{1}{\sqrt{\gamma(t)}}. \tag{8}$$

Furthermore, near the blow-up time ($\gamma \gg 1$), for fixed $r \neq 0$ we have $\sqrt{\gamma} r \gg 1$ and

$$u(r) \approx \frac{1}{\gamma r^4}. \tag{9}$$

2.3. The outer region

Away from the core region, as $t \to T$, $u(r,t)$ approaches a function $u(r,T) = \psi(r)$ where $\psi(r)$ is finite and defined for all $r > 0$. It is shown in [2] that *for r small* but bounded away from zero (viz., $L(t) < r \ll 1$), as $t \to T$

$$\psi(r) = \psi_0(r)(1 + \mathcal{O}(1)) \equiv C \frac{\exp(-2\sqrt{\log(1/r)})}{r^2}(1 + \mathcal{O}(1)) \quad \text{as } r \to 0, \tag{10}$$

where C is an appropriate constant. It is important to note that this outer region solution (10), illustrated in Fig. 2, is time independent.

Note that ψ_0^β (and hence the function ψ^β) is integrable over $\mathbb{R}$ *only if* $\beta \leqslant 1/2$, and specifically,

$$\int_0^\infty \psi_0 \, r \, \mathrm{d}r = C(1 + \mathcal{O}(1)) \quad \text{and} \quad \int_0^\infty \psi_0^{1/2} \, \mathrm{d}r = 4C^{1/2}. \tag{11}$$

2.3.1. Matching the core and outer regions

A crucial feature of the solution behaviour is that the inner solution (7) does not match smoothly with the outer solution $\psi(r)$ at any range. Indeed, if r/L is large then the inner approximation of u is $1/\gamma r^4$ (but is

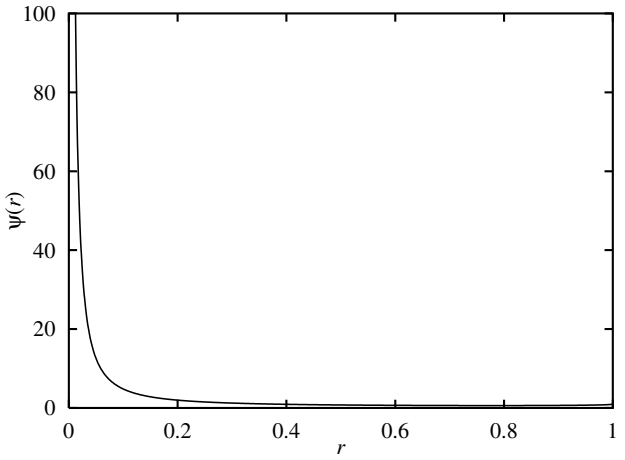

Fig. 2. The behaviour of u in the outer region where it approximates $\psi_0(r)$.

time dependent). On the other hand, since $\log(1/r)$ is slowly varying for small r, the outer solution is *roughly* proportional to $\psi_0(r) \propto \frac{1}{r^2}$ (and is time independent). Therefore, there is no match between inner and outer solutions at any range. This is in contrast to many parabolic blow-up problems and the nonlinear Schrödinger equation where the core solution evolves to a time independent function which smoothly matches with an outer solution.

The inner and outer approximations of $u(r,t)$ are *of comparable size* when r satisfies the relation

$$\frac{C\,\mathrm{e}^{-2\sqrt{\log(1/r)}}}{r^2} \approx \frac{1}{\gamma r^4}.$$

Rearranging, this gives

$$C\,\mathrm{e}^{-\sqrt{2}\sqrt{\log(1/r^2)}} r^2 \approx K^2(T-t)\mathrm{e}^{-\sqrt{2}\sqrt{\log(1/(T-t))}}.$$

Solving for the location of the transition $r = r^*(t)$ from the core to outer region,

$$r^*(t) \approx \frac{K}{\sqrt{C}}\,(T-t)^{1/2}. \tag{12}$$

Note that $r^*(t) \gg L(t)$ so that the transition occurs at a value of r which is large compared to the natural length-scale of the core region.

In conclusion, the results of [2] imply that provided the time t is close to the blow-up time T so that the effects of the initial conditions are small, for $r < r^*(t)$ the solution $u(r,t)$ is well approximated by (7) and for $r^*(t) < r \ll R$ by (10). For values of r of the order of R (i.e. close to the boundary), neither description will be accurate due to the effects of the boundary terms.

For illustration, in Fig. 3, we show a snapshot of the actual solution of (1) computed using the numerical method described in the next section and terminating when $\gamma = 1.578 \times 10^{21}$, together with its inner and outer solution approximations. For this case the inner and outer solution approximations coalesce near $r^* = 1.27 \times 10^{-9}$ given by (12). As can be observed from the figure, the inner and outer solutions closely match the actual solution except near $r = R = 1$ where the asymptotic formulae break down due to the effect of the boundary conditions.

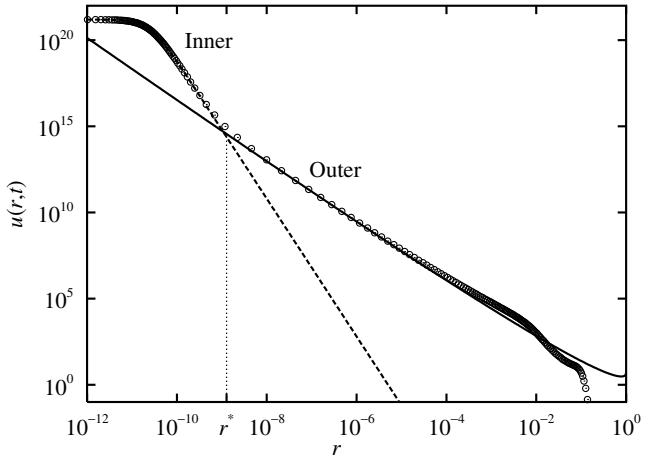

Fig. 3. Typical behaviour of $u(r,t)$ near the blow-up time T computed from numerical integration of (1) using an adaptive mesh technique (see below). The solution is well approximated by $\bar{u}$ in the inner region and by ψ_0 in the outer region away from the boundary $r = R = 1$.

3. Numerical evidence for the blow-up asymptotics in [2]

3.1. The numerical method

As remarked, it is not clear whether the asymptotic description of the solution given in [2,11] and the previous section describes the behaviour for general initial data. A first objective here is to give some numerical support to the conjecture that this asymptotic description represents an attracting solution for a significant set of initial data. The numerical challenge is severe. To compare the approximately self-similar asymptotic description given in [2] with a true self-similar formula it is necessary to compute the solution to the point at which the error terms in the asymptotic formulae of the form $1/\sqrt{\log(T-t)}$ are small. To do this it is necessary to compute solutions which are very large (of the order of 10^{22}) and which evolve on very small length scales (of the order of 10^{-11}). To perform such numerical computations it is essential to use an adaptive procedure in which mesh points are clustered close to the region where the singularity develops. There are various procedures for doing this, including h-refinement where mesh points are successively added in the singular region and r-refinement where a (fixed) number of mesh points are moved into the region. Following the success of the methods for parabolic blow-up described in [12], we consider an r-refinement method where the mesh points evolve according to a moving mesh PDEs (MMPDE).

We solve the system (1) in a radially symmetric setting (i.e., effectively integrating a system of equations in 1D) using MOVCOL [13], a moving method of lines code based upon a moving collocation method. The physical PDEs are discretised in space on a non-uniform mesh with a cubic Hermite collocation-type method, and the MMPDEs are discretised in computational space with a 3-point finite difference method.

The resulting system of ODEs is integrated with the code DASSL [26] which is designed to solve stiff differential-algebraic equations (DAEs) of the form $g(t,y,\mathrm{d}y/\mathrm{d}t) = 0$ by combining variable order backward differentiation algorithms with the numerical linear algebra routines from LINPACK [27].

More specifically, the (moving) mesh points are $X_i(t) = X(i/N,t) \in [0,R]$ where $X(\xi,t)$ is a transformation from a fixed *computational* coordinate ξ to the moving frame. The function $X(\xi,t)$ evolves during the calculation to cluster the mesh points close to the singularity, and the basic adaptive method involves solving the physical PDE and an MMPDE for $X(\xi,t)$. For each time level t we compute a coordinate transformation $X(\xi,t)$:$[0,1] \to [0,R]$. The standard criterion for computing $X(\xi,t)$ in one dimension is the equidistribution of a monitor function $M(r,t) = M(u(r,t))$ measuring the difficulty in describing the solution u at (r,t) (i.e., where more mesh points are needed to smoothly extrapolate the solution). Typical choices of monitor function involve a combination of the size of the solution and its steepness. The equidistribution of the monitor function in integral form reads

$$\int_0^X M(u)\,\mathrm{d}r = \xi \int_0^R M(u)\,\mathrm{d}r \tag{13}$$

and its differential form

$$(M(u)X_\xi)_\xi = 0. \tag{14}$$

With the MMPDE approach, one does not try to solve (14) exactly. There are a variety of choices for the time dependent MMPDE which one solves instead, and for much the same reasons as in [12] (see below) we use MMPDE6 [14,15], which is

$$-X_{\xi\xi t} = \frac{1}{\tau}(M(u)X_\xi)_\xi. \tag{15}$$

In practice, there are several advantages of not solving (14) exactly, viz., (a) a simple initial mesh such as a uniform one can often be chosen, (b) more stable meshes with reduced risk of mesh crossings are generated, and (c) the possibility of over-concentrating points in the singular regions and depleting the mesh points elsewhere is reduced.

MOVCOL numerically integrates the discrete collocations equations for the PDEs (1) expressed in the *mesh coordinates* and the discrete finite difference equations for (15) simultaneously [13]. Roughly speaking, the method works by suitably choosing M to be large at points where the solution has a singular form. The advantage of the formulation (15) is that M can be chosen to balance the temporal and spatial scalings of the solution.

The resulting process evolves the solution and the mesh on a combined manifold corresponding to an *equidistributed* solution/mesh.

If equidistribution is enforced too rigidly then DASSL warns that the resulting equations are very *stiff*. Stiffness generally indicates a wide difference in time scales for the equations being integrated, and short time steps chosen due to the presence of the shorter time scales prevents efficiently following the solution in the longer ones, particularly when the short time scales describe transient effects which become unimportant [28]. For the chemotaxis system studied here, this stiffness difficulty has turned out to be problematic, causing the solution process to slow down and even freeze. A study of the precise cause of this stiffness and its effect for a code like DASSL which is designed to efficiently handle stiff problems, while an important practical matter to pursue in understanding the general MMPDE approach, lies outside the scope of this paper and requires further investigation.

On the other hand, if equidistribution is enforced too weakly (e.g., if the mesh evolves too slowly) then the mesh will not adapt quickly enough to the solution and resolution will be lost (as there is insufficient adaptivity to resolve the blow-up). With an optimal 'scale invariant' method the rate at which the solution evolves onto the equidistribution manifold is of the same order as the overall rate of evolution of the solution. Choosing the monitor function correctly, the MMPDE scales properly and the problems with stiffness in the solution are avoided. We see later that an optimal choice of monitor function M from the joint perspectives of mesh regularity and overall ease of computation is

$$M(u) = u^{1/2}. \tag{16}$$

In the next section we will return to the motivation for this choice of monitor function.

3.2. Initial conditions and other numerical parameters

We briefly summarise the numerical results obtained when solving (1) using MOVCOL (with double precision) and (16). These results are all consistent with the asymptotic analysis of [2]. For all our computations we take the Gaussian initial data

$$u(r,0) = 1000\,\mathrm{e}^{-500r^2},$$
$$v(r,0) = 10\,\mathrm{e}^{-500r^2},$$

over the domain [0,1].

This leads to solutions which become singular in a finite time T ($T \approx 5.15 \times 10^{-5}$).

For the 2D computations, the particular choice of initial conditions is not crucial to test the asymptotics, provided that the initial mass of u is large enough to drive blow-up [29,30]. However, the blow-up time T depends dramatically on the specific choice of initial conditions. An almost flat initial configuration leads to a considerable increase of the blow-up time while maintaining the asymptotic form of the solution.

Interestingly, in 3D blow-up will occur regardless of the initial mass. However, the type of blow-up does depend on the initial configuration, and blow-up can occur in a self-similar manner or in a way which corresponds to imploding ring-waves [23].

We typically use fewer than 250 mesh points, smoothing parameter $\tau = 10^{-10}$ and no spatial smoothing with a moving mesh method of the form MMPDE6 (15) (see [14,15] for details).

The computations are performed on a Linux platform with a Xeon 2.2 GHz processor and 1 Mb RAM. Typical computations take approximatively 40 CPU seconds (10 s for initial setup and initial equidistributed mesh, and 30 s for the remainder of the run until collapse of the solution induces a stepsize error in the differential algebraic equation solver due to stiffness).

As a check of the accuracy of the numerical computation, during the run we compute the mass of the solution $u(r,t)$ as given by (2). We can then verify that it is conserved to within some tolerance level. Indeed, even for times very close to blow-up the error in the mass, with respect to the initial mass, is found to be smaller than 0.7%.

Fig. 4 depicts the time evolution of $u(x,t)$ for a typical run using the above setup.

3.3. Calculation of the blow-up time T

The blow-up time T is estimated to high precision by computing until $u(0,t^*) \approx 10^{21}$ and approximating T by t^*. As an indicator of the validity of the numerical results we compare the computed blow-up time T as a function of the number of mesh points N (see Fig. 5). For the wide range of N values we consider, the blow-up time remains relatively constant: $5.115 \times 10^{-5} < T < 5.118 \times 10^{-5}$, i.e., a variation of approximatively 0.05% (for $300 < N < 700$ the variation is approximatively 0.01%). Obtaining consistency can be a source of some numerical difficultly, e.g. in Fig. 13 of [1] T appears to vary logarithmically as a function of N.

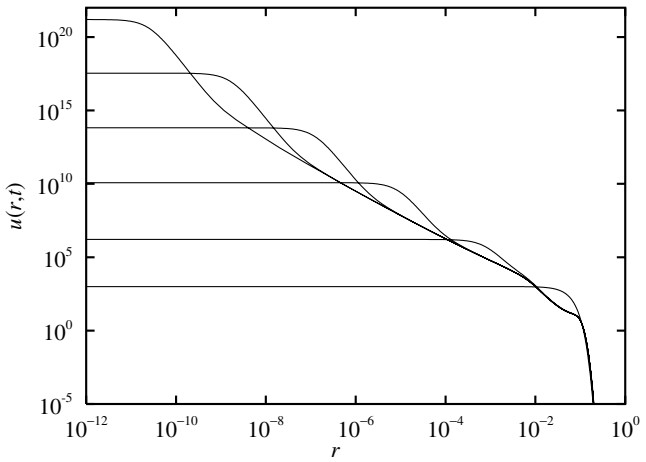

Fig. 4. Time evolution of blow-up solutions using the moving mesh method. From bottom to top: $T - t \approx T$ (initial condition $t = 0$), 1.85×10^{-6}, 1.53×10^{-9}, 1.07×10^{-12}, 5.67×10^{-16}, 2.98×10^{-19}. Here, Blow-up time is approximately $T = 0.51174514141272323369 \times 10^{-4}$.

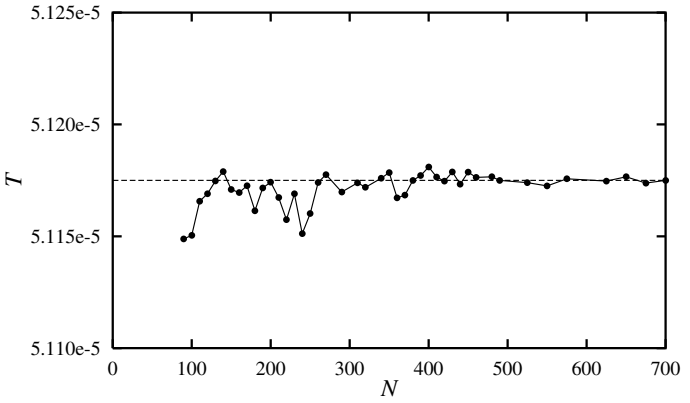

Fig. 5. Blow-up time T as a function of the number of mesh points N used for the moving mesh method.

3.4. Temporal behaviour of u(0,t)

From (4), we have that

$$T - t = (K^2 u(0,t))^{-1/(1+2\alpha)}(1 + \mathcal{O}(\log(\tau)/\sqrt{\tau}), \quad \text{with } \tau = -\log(T-t)$$

or similarly that

$$u(0,t) = \frac{\tilde{K}}{(T-t)^{1+2\alpha}}(1 + \mathcal{O}(\log(\tau)/\sqrt{\tau}), \tag{17}$$

with $\tilde{K} = 1/K^2$, so that if (4) represents the true asymptotic behaviour then

$$u(0,t)(T-t)e^{\sqrt{2}(-\log(T-t))^{-\frac{1}{2}}} \to \tilde{K} \quad \text{as } t \to T. \tag{18}$$

The formulae (17) and (18) only become asymptotically sharp when $\log(u(0,t))$ is large so that $1/\sqrt{\tau}$ is small. This imposes a severe restriction on the numerical method, which is required to compute very large solutions. Unfortunately, the numerical calculations become dominated by rounding (and other) errors when u is too large and when $(T-t)$ is too small. We find our numerical calculations to be reliable and the asymptotic formulae observable for $10^{-20} < (T-t) < 10^{-5}$. Over this range, α given in (17) varies from approximately 0.1–0.2 (cf. Fig. 6).

It should be emphasised that this is a relatively small variation given that the other terms in (17) are changing by more than ten orders of magnitude, making it very hard to distinguish between the logarithmic law (18) and a power law, although both can be distinguished from a self-similar type of evolution with $\alpha = 0$. A representative value of α over this range, say

$$\alpha = 0.15, \tag{19}$$

appears to be a reasonable approximation to use, leading to approximately power law behaviour

$$u(0,t) \approx \frac{\tilde{K}}{(T-t)^{1.3}}.$$

The growth in $u(0,t)$ predicted by this analysis is compared with the numerical results from calculating $u(0,t)$ in Fig. 7, where we plot $\log(u(0,t))$ against $\log(T-t)$. Here, T is first estimated to high precision using the procedure described above. We show the results for both a 2D domain ($d = 2$) with $M(u) = u^{1/2}$ and a 3D domain ($d = 3$) with $M(u) = u$. (The choice of M is justified in the next section). For $d = 3$ the solution

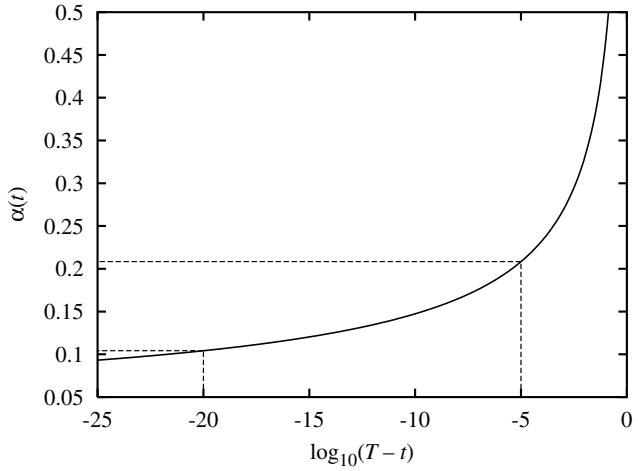

Fig. 6. The behaviour of $\alpha(t)$ as the blow-up time T is approached.

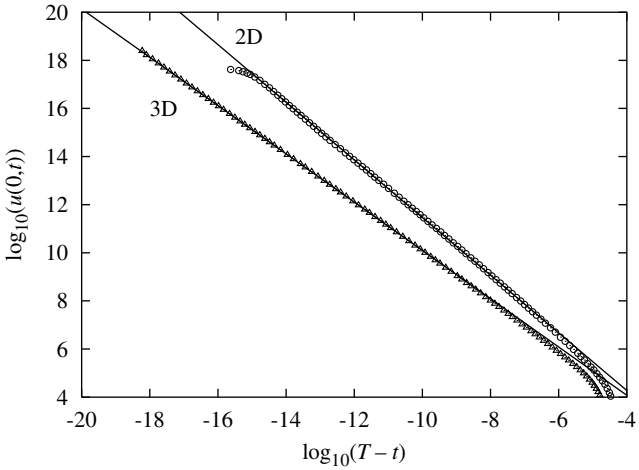

Fig. 7. The form of $u(0,t)$ near to the blow-up time T. Blow-up for 3D is self-similar with exponent -1. For 2D there is no true self-similar blow-up but a power law is observed with α roughly between 0.1 and 0.15 in an asymptotic range for $T - t > 10^{-15}$.

has a true self-similar form with $u(0,t) \sim (T-t)^{-1}$, and since the difference between approximate and true self-similar behaviour is more easily determined, we can be reasonably sure that we are not observing a numerical artifact.

Over the range of values of $(T-t)$ for which there are both reliable numerical computations and sharp asymptotic results, both of the curves in Fig. 7 are close to straight lines. For the 2D case this is due to the slow variation in α over this range, where the line has a gradient close to -1.2. This corresponds to a power law of $(1+2\alpha)$ and is consistent with a value of α between 0.1 and 0.15.

For the 3D case, the line has the 'self-similar' gradient of -1, consistent with the growth of the approximate self-similar solution. For the non-self-similar solutions corresponding to imploding shock waves, analysed in [23], an argument is given which suggests that they are stable. Investigations employing the numerical techniques described in this manuscript are currently underway in [31] to examine this issue.

3.5. Spatial structure of $u(r,t)$

As a second test of the asymptotic formulae, we examine the spatial structure of $u(r,t)$, viz., how the natural length scale $L(t)$ varies with $(T-t)$. Following [1], we estimate $L(t)$ from the numerical computations by finding the value of r at which $u(r,t) = u(0,t)/5$. According to (7) this occurs asymptotically when $r = L(t)\sqrt{\sqrt{5}-1}$. From (5), we expect to see

$$\frac{L}{\sqrt{T-t}} = K(T-t)^{\alpha}\left[1+\mathcal{O}\left(\frac{\log(\tau)}{\sqrt{\tau}}\right)\right].$$

In Fig. 8, we present two calculations to support the above estimate. In the top of the two figures we plot L as a function of $(T-t)$. This graph clearly indicates that L scales in a manner close to $\sqrt{T-t}$. More careful analysis of this calculation is given in the bottom plot where $L/\sqrt{T-t}$ is plotted as a function of $T-t$. Here we see that $L/\sqrt{T-t}$ is not constant but is slowly varying. The solid line on this graph gives the correction term $K(T-t)^{\alpha}$ as predicted by Herrero and Velázquez [2]. It is evident that the numerical results approach this term as $(T-t)\to 0$. Over the range of values plotted on the graph, $\tau = -\log(T-t)$ varies from about 11 to 40, so that the value of the error bound $\log(\tau)/\sqrt{\tau}$ varies from 0.72 to 0.57. The good convergence of the numerical scheme indicates that this error bound may not be optimal. Self-similar blow-up for $\alpha = 0$ would correspond to $L \propto \sqrt{T-t}$ which is certainly not observed.

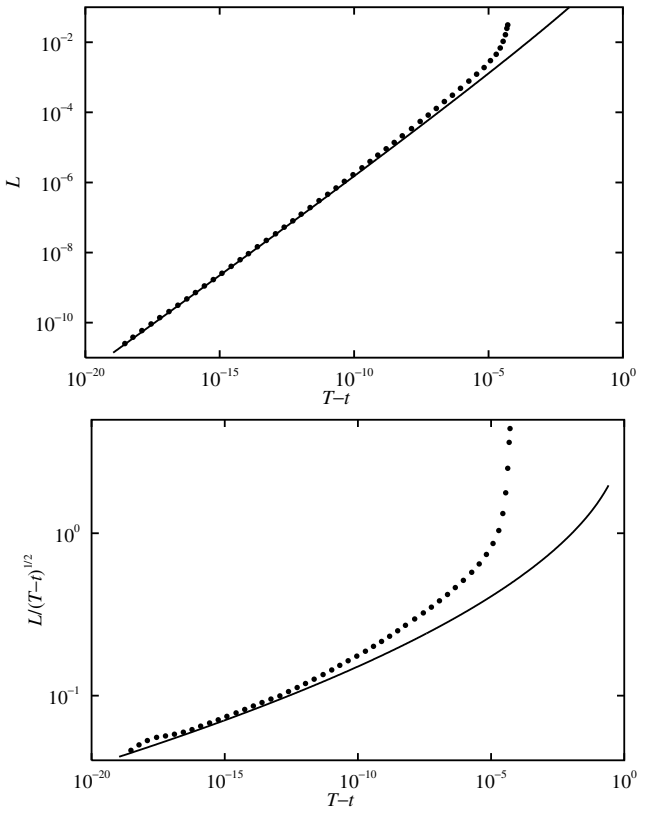

Fig. 8. Corroboration of logarithmic correction due to near-self-similar blow-up. Top plot depicts L as function of time to blow-up $T-t$. Bottom plot depicts $L/\sqrt{T-t}$ which is constant for strict self-similar blow-up. Dots correspond to numerical simulations obtained using moving mesh method, and solid lines correspond to *non-self-similar* asymptotics predicted in [2].

It is crucial to use a reliable integration technique in order to observe the proper solution asymptotics. In [1] a second-order finite-difference method in space with adaptive time and mesh refinement is used to compute a similar graph to the above, where their mesh refinement is implemented such that mesh points are drawn into the inner core whenever the maximum density increases by 1%. Even using this mesh refinement method, though, there is difficulty detecting the logarithmic correction of the α exponent in (5) as in this paper their numerical estimates of $L/\sqrt{T-t}$ approach a constant value near blow-up – so that the characteristic length L appears to behave in a self-similar manner. Well aware of the numerical difficulties in detecting the logarithmic corrections for approximately self-similar blow-up, they left the numerical verification of the solution in [2] as an open problem (see also [11]). We are able to capture the logarithmic correction with a suitable choice of the monitor function for our moving mesh method, and below we see the effect of various choices of monitor functions.

4. Mesh calculation

4.1. Form of monitor function

To analyse the remeshing procedure using MMPDE6 to solve the 2D and 3D chemotaxis problem (1), we look first at mesh regularity and then at the ease of solution of the resulting system of ODEs for the optimal monitor functions. Using the results of [2], we estimate the analytic form of the mesh and compare the resulting meshes with numerically computed ones.

When updating the mesh close to the collapse time it is essential that the mesh points do not move too fast; otherwise, the resulting system of equations is very stiff. Nevertheless, the mesh points must not move too slowly or they will not track the singularity. Ideally, they should evolve at the same rate as the underlying solution. To achieve this balance, the monitor function must scale correctly in a *temporal sense*. Specifically, if μ is a natural time scale and L a natural length scale then the left hand side of MMPDE6 scales as L/μ and the right-hand side as LM, so they balance if $M \sim 1/\mu$. As collapse is approached, a natural time scale for the formation of the singularity is $\mu = (T-t)$. Hence, to evolve the mesh points at the correct timescale, the monitor function M must satisfy the identity

$$M(u) = (T-t)^{-1}.$$

For the chemotaxis problem this can be achieved if we use monitor functions of the form

$$M(u) = u^{\beta} \equiv u^{1/(1+2\alpha)}. \tag{20}$$

These functions both have good scaling properties and are easy to use during the computations. Taking $\alpha = 0.5$ in (20) leads to the estimate $\beta = 0.5$, so that

$$M(u) = u^{1/2}. \tag{21}$$

We see later that this choice leads to a robust method.

If in contrast we take $\alpha = 0.15$, determined previously as being a good approximation over the asymptotic range, then

$$M(u) = u^{0.77}. \tag{22}$$

We find later that while it does place the mesh points correctly, it tends to lead to stiff equations in the initial phase of mesh placement.

As α is slowly decreasing, we have $\beta \geqslant 1/2$ and asymptotically $\beta = 1$. The latter choice gives

$$M(u) = u, \tag{23}$$

which is appropriate for numerically capturing the solution evolution for problems in 3D.

4.2. Mesh evolution for $M = A + u^{\frac{1}{2}}$

To construct a mesh distribution process such that both (a) the mesh adapts to the solution blow-up behaviour and (b) there are a sufficient number of mesh points in both the core and outer regions, we follow [32] and instead of (20) use a regularised monitor function given by

$$M(u) = A + u^{\beta}, \quad A, \beta \geqslant 0. \tag{24}$$

The constant A is insignificant close to the singularity and allows for a more uniform distribution of mesh points near the boundary. In this subsection we analyse the case $\beta = 1/2$, which is essentially optimal in striking a balance between satisfying criterion (b) and giving non-stiff mesh equations. While not quite optimal in resolving the singularity, it still does fairly well over the asymptotic range. In our analysis we shall assume that the mesh is perfectly equidistributed.

4.2.1. Calculating the right hand side of (13)

The right hand side of the integral in (13) in this case is

$$\xi\left[AR + \int_0^R u^{1/2}\,\mathrm{d}r\right].$$

To evaluate this integral we consider the two expressions for u over the core and outer regions.

4.2.1.1. The core region. Here u is scale-invariant and from (7) evolves in the manner

$$u(r,t) = \frac{1}{L^2}\bar{u}\left(\frac{r}{L}\right), \quad L^2 = 1/\gamma, \quad \gamma = u(0,t).$$

Comparing $\bar{u}$ with ψ_0 it is reasonable from (12) to assume that the inner (core) region can be extended to the point

$$r^* = \frac{\Lambda}{\sqrt{\gamma}},$$

where Λ is taken to be large. Using the expression for u in the core region we then have

$$\int_0^{r^*}\left(A + u^{1/2}\right)\mathrm{d}r = Ar^* + \int_0^{r^*}\frac{1}{L}\left(\frac{\mathrm{d}r}{1 + r^2/L^2}\right) = Ar^* + \tan^{-1}\left(\frac{r^*}{L}\right) \to AL^* + \frac{\pi}{2} \quad \text{as } \Lambda \to \infty. \tag{25}$$

4.2.1.2. The outer region. Here $u(r)$ is well approximated by $\psi(r)$ when r is small. Since $\psi^{1/2}$ is integrable, for some constant D

$$\int_{L^*}^{R} A + u^{1/2}\,\mathrm{d}r \approx A(R - L^*) + \int_0^R \psi^{1/2}\,\mathrm{d}r \equiv A(R - L^*) + D.$$

Combining these results, we conclude that regardless of the level of blow-up and size of $L(t)$, in the singular limit the right hand side of (13) simply evolves towards a constant, viz., we have approximately

$$\int_0^R M\,\mathrm{d}r = AR + \frac{\pi}{2} + D. \tag{26}$$

4.2.2. Calculating location of mesh points

The second mesh criterion consists of *roughly* distributing the mesh points equally between the core and outer regions: we call it the "50:50 condition". This condition must be satisfied

to give a smooth and more regular mesh. We can gauge the mesh by how well this condition is satisfied.

We again consider the core and outer regions separately.

4.2.2.1. The mesh in the core region. From (13) and (26), in the core region

$$\int_0^X M\,\mathrm{d}r = AX + \tan^{-1}(X/L) = \xi(AR + \pi/2 + D).$$

In the case $A = 0$ this gives

$$X(\xi,t) = L(t)\tan(\xi(\pi/2 + D)), \tag{27}$$

provided that

$$\xi(\pi/2 + D) < \pi/2 \quad \text{so that } \xi < 1/(1 + 2D/\pi). \tag{28}$$

From (27), the meshing procedure thus places $1/(1 + 2D/\pi)$ of the mesh points within the core region at a spacing proportional to L. As $\xi \to 1/(1 + 2D/\pi)$, we have $X/L \to \infty$, implying that the mesh points leave the core region at this point.

4.2.2.2. The mesh in the outer region. Assuming that X/L is *large* but that X itself is *small*, from (26) we have

$$\int_0^X M\,\mathrm{d}r = AX + \pi/2 + \int_0^X \psi^{1/2}(r)\,\mathrm{d}r = \xi(AR + \pi/2 + D).$$

Approximating $\psi(r)$ for small r by $\psi(r) \approx \psi_0(r) = C\,\mathrm{e}^{-2\sqrt{\log(1/r)}}/r^2$, for small X we thus have

$$s(X) + AX + \pi/2 = \xi(AR + \pi/2 + D), \tag{29}$$

where

$$s(X) \equiv \int_0^X \psi_0^{1/2}(r)\,\mathrm{d}r = 2\sqrt{C}\left[\sqrt{\log(1/X)} + 1\right]\mathrm{e}^{-\sqrt{\log(1/X)}}. \tag{30}$$

Examining this mesh for $A = 0$, if we assume that the asymptotic description of $\psi(r) \approx \psi_0(r)$ remains valid up to $r = R$ then

$$D = \int_0^R \psi^{1/2}\,\mathrm{d}r \approx \int_0^R \psi_0^{1/2}\,\mathrm{d}r = s(R), \tag{31}$$

so that

$$s(X) + \pi/2 \approx \xi(\pi/2 + D) \quad \text{so that } s(X) = \frac{\pi}{2}\left[\xi\left(1 + \frac{2D}{\pi}\right) - 1\right]. \tag{32}$$

The function $s(X)$ is monotone increasing and tends to 0 as $X \to 0$. Thus, the mesh points only lie in the outer region if $\xi > 1/(1 + 2D/\pi)$, which is consistent with the earlier calculation.

We summarise these results in the following lemma.

Lemma 1. *Using $M(u) = u^{1/2}$ in MMPDE6, (i) the core region is described by the values of the computational variable for which $\xi < 1/(1 + 2D/\pi)$. In this region*

$$X(\xi,t)/L = X(\xi,t)u(0,t)^{1/2} = \tan(\xi(\pi/2 + D)),$$

where D is a constant. (ii) The outer region is described by values of the computational variable for which $\xi > 1/(1 + 2D/\pi)$. In this region

$$s(X) = \frac{\pi}{2}\left[\xi\left(1 + \frac{2D}{\pi}\right) - 1\right],$$

with $s(X)$ *given by* (30).

Note that regardless of the value of $T - t$, a *fixed proportion* of the mesh points are placed in the core region, so the 50:50 condition is satisfied.

In Fig. 9, we plot the computed scaled mesh in the core region. It is clear that X/L becomes unbounded around $\xi = 1/(1 + 2D/\pi) = 0.3242$. We estimate D by approximating $\int_0^R M(r)\mathrm{d}r$ and plot the analytic core mesh predicted from (27). For the resulting approximation $D = 3.274$ shown in Fig. 9, we see good agreement between these two meshes.

In Fig. 10, we compare the computed mesh $X(\xi)$ in the outer region with the analytic mesh determined using the above value of D. Observe that $X \to 0$ as ξ decreases towards $\xi = 0.32$, which is consistent with the core region calculation. This shows the good agreement between the mesh in the outer region calculated using MMPDE6 and the outer region approximation (32).

A plot comparing the computed mesh and the predicted mesh over the whole interval is given in Fig. 11. Here the change between the core and the outer region is very clear. Overall the analytic approximation of the mesh is very good away from the boundary at $r = R = 1$.

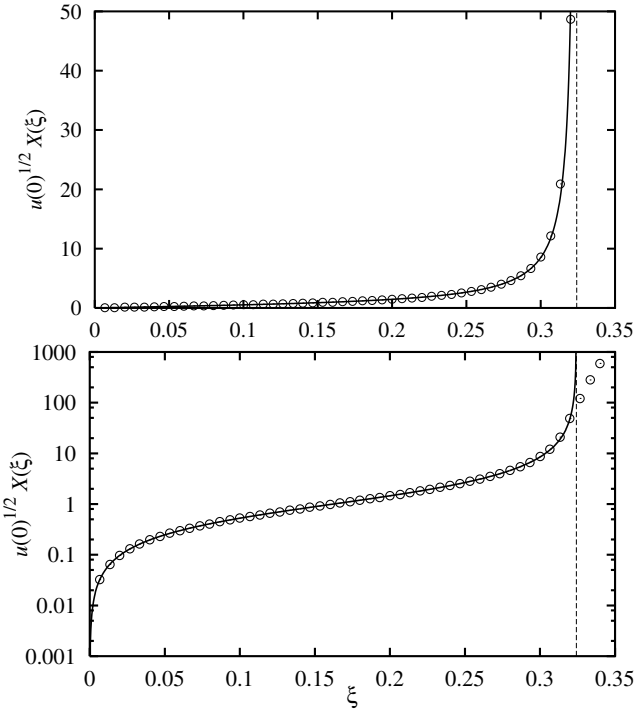

Fig. 9. Mesh computed in the core region. The data (circles) represents numerical computations using MMPDE6, and the fitted curve is provided by the inner region approximation (27) with $D = 3.274$. We use 151 mesh points and $T - t$ is approximately 10^{-16}. Top: linear–linear, bottom: linear–log.

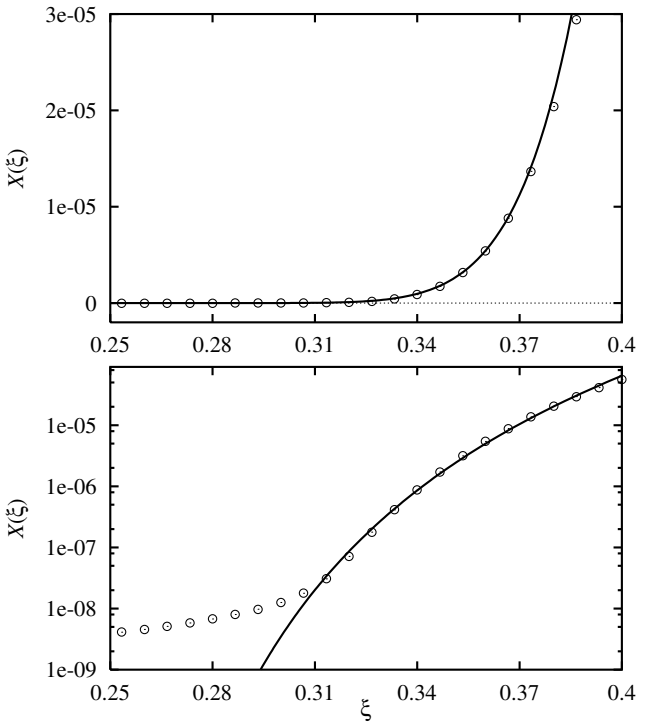

Fig. 10. The computed mesh for the outer region. The data corresponds to numerical results obtained using MMPDE6 and the fitted curve represents the outer approximation (32). Top: linear–linear, bottom: linear–log.

4.3. Mesh evolution for $M = A + u^\beta$, $\beta > 0$

Consider the class of general monitor functions $M = A + u^\beta$ for $\beta > 0$. Defining $I_1(X)$ as the integral of u^β in the core region,

$$I_1(X) = \int_0^X u^\beta \, \mathrm{d}r = \int_0^X \frac{1}{L^{2\beta}} \bar{u}(r/L)^\beta \, \mathrm{d}r = \frac{1}{L^{2\beta-1}} \int_0^{X/L} \bar{u}(y)^\beta \, \mathrm{d}y. \tag{33}$$

If $\beta > 1/4$ then $\bar{u}^\beta$ is integrable over $\mathbb{R}$, in which case this inner integral tends towards

$$I_1(\infty) = \frac{N}{L(t)^{2\beta-1}}$$

for an appropriate constant N. This implies the following.

Lemma 2. *(a) If* $1/4 < \beta < 1/2$ *then* $I_1(\infty) \to 0$ *as* $L(t) \to 0$. *(b) If* $\beta > 1/2$ *then* $I_1(\infty) \to \infty$ *as* $L(t) \to 0$.

The contribution to the total integral in (13) from the outer region has the form

$$I_2 = \int_L^R \psi^\beta \, \mathrm{d}r \approx \int_L^1 \frac{C^\beta \mathrm{e}^{-2\beta\sqrt{\log(1/r)}}}{r^{2\beta}} \, \mathrm{d}r.$$

So if $\beta < 1/2$, I_2 is both finite and bounded away from 0 as $L(t) \to 0$, say $I_2 = E$. If $\beta > 1/2$, I_2 scales as $L(t)^{1-2\beta}$, and the contribution to the overall integral from the outer region is simply proportional to the contribution from the core region. We have

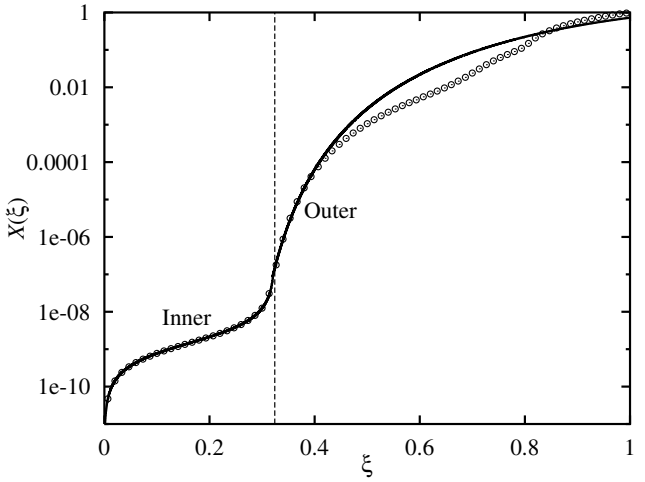

Fig. 11. Mesh transformation for entire domain Ω. Vertical dashed line separates inner and outer regions. The data corresponds to numerical results obtained by integrating (1) using MMPDE6. Solid curve consists of inner (27) and outer (32) approximations.

Lemma 3. (*a*) *If* $\beta < 1/2$ *then* $I_1(\infty)/I_2 \to 0$ *as* $L(t) \to 0$. (*b*) *If* $\beta > 1/2$ *then* $I_1(\infty)/I_2 \to H$ *as* $L(t) \to 0$, *where* H *is a constant.*

4.3.1. The case $\beta < 1/2$

In this case, it follows from (33) that

$$\int_0^1 M(u)\mathrm{d}r = L^{1-2\beta}F(\infty) + E,$$

where $F(y) = \int_0^y \bar{u}^\beta \,\mathrm{d}y$. In the core region the mesh is given by solving the equation

$$L^{1-2\beta}F(X/L) = \xi(L^{1-2\beta}F(\infty) + E),$$

so that

$$F(X/L) = \xi(F(\infty) + L^{2\beta-1}E).$$

This expression is valid only if

$$\xi(F(\infty) + L^{2\beta-1}E) < F(\infty),$$

giving

$$\xi < \frac{1}{1 + L^{2\beta-1}E/F(\infty)} \approx \frac{F(\infty)}{E}L^{1-2\beta}.$$

We see that as $L \to 0$ the proportion of mesh points placed in the core region becomes vanishingly small. Hence, the mesh will *freeze* and the solution will not be well resolved. In practice, the method does not behave too badly in the initial stages of the evolution, but for large values of u the whole system has *spurious oscillations*.

4.3.2. The case $\beta > 1/2$

The integral in the core scales as $L^{1-2\beta}$, and the integral in the outer region scales in *exactly* the same way. As a consequence, we obtain a 50:50 mesh for values of $\beta \geqslant 1/2$. The analysis for the mesh location is then similar to that in the last subsection.

4.4. Solution of resulting ODEs

To be most effective the computed mesh should have the 50:50 property and scale well with time. We have shown that the monitor function u^β has the first property provided that $\beta \geqslant 1/2$. However, in order for the mesh to scale asymptotically with time the proper choice for β is $\beta = 1/(1 + 2\alpha)$.

We investigate the effect of using the general form for the monitor function (24) in the moving mesh equation (15) in the case $A = 0$ for simplicity, where MMPDE6 becomes

$$-X_{\xi\xi t} = \frac{1}{\tau}(u^\beta X_\xi)_\xi. \tag{34}$$

From (17), at the solution's maximum value

$$u(0,t)^\beta = \frac{1}{L(t)^\beta} = \frac{\tilde{K}^\beta}{(T-t)^{\beta(1+2\alpha)}}.$$

The natural time-scale for the evolution of the whole system, viz., the amount of time before blow-up occurs, is $1/(T - t)$, and hence relative to the natural time-scale the right hand side of (34) has magnitude

$$\frac{1}{\tau}(T-t)^{\beta(1+2\alpha)-1}.$$

If $\beta(1 + 2\alpha) \approx 1$ then the mesh achieves the goal of evolving at the same rate as the solution. If $\beta(1 + 2\alpha) > 1$ then the mesh evolves more rapidly than the solution, and the ODEs for the mesh evolution are stiff. In the early stages of the system evolution, α takes larger values than later on. Thus, if β is too large initially then the mesh ODEs will be too stiff to solve easily. Of the values of β that give 50:50 meshes, $\beta = 1/2$ leads to the least stiff equations and is in this respect an optimal choice.

Fig. 12 shows a series of double precision calculations of u using $M = A + |u|^\beta$. The top and bottom plots depict the maximum height of the solution $u(x,t)$ before the numerics break down, as a function of β and A for $A = 1$ and $\beta = 0.5$, respectively. This maximum value gives a crude measure of the robustness of the numerical scheme. In the figure the circles correspond to break down of the computations caused by a lack of points in the core region, which produces time-oscillations in the height of the aggregate. In contrast, the crosses correspond to a break down of the computations due to stiffness of the time integration procedure causing a halt (failure to converge with the prescribed accuracy) in the differential algebraic system solver DASSL [26]. It is clear that $\beta = 1/2$ gives the best results, at least for the early and intermediate stages of the computations. Interestingly, although taking $A > 0$ leads to a smoother mesh close to the boundary at $r = R$, it leads to less robust computation.

More specifically, for A close to zero there are enough points in the core region but eventually the numerics break down because DASSL indicates that the equations have become too stiff. On the other hand, for larger A there are not enough points kept in the core region so that the loss of resolution triggers time-oscillations of the solution (see Fig. 15).

4.5. Choice of τ

Whilst the value $\beta = 1/2$ is optimal when the solution is large enough ($\alpha < 1/2$), the mesh asymptotically evolves more slowly than the solution. This effect can be somewhat mollified by using appropriate values

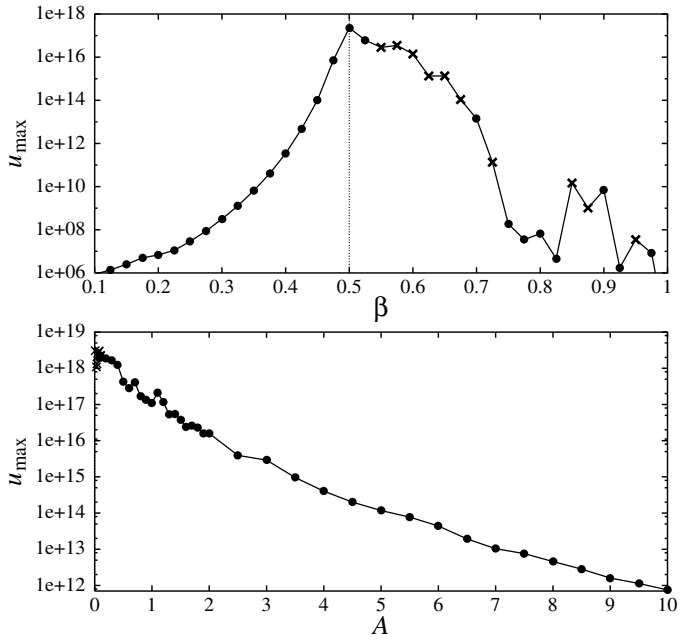

Fig. 12. Performance of the monitor function $M = A + |u|^{\beta}$. The top and bottom plots depict the maximum height ($u_{\max}$) of the solution $u(x,t)$ before the computation breaks down. Top: $u_{\max}$ as a function of β for $A = 1$. Bottom: $u_{\max}$ as a function of A for $\beta = 0.5$. The numerics break down due to depletion of mesh points in the core region (circles) or due to stiffness (crosses).

of τ *in this range*. Specifically, if (17) holds then the mesh will evolve at the correct time scale provided that

$$\tau = (T-t)^{1/2-\alpha}. \tag{35}$$

From the definition of α, $\log(T-t) = -\frac{1}{2\alpha^2}$, so eliminating $(T-t)$ from (34) and (17), we have $\alpha^2 \log(\tau) = (\alpha - 1/2)/2$ and $\alpha^2 \log(u(0,t)) = \log(\tilde{K})\alpha^2 + (1+2\alpha)/2$. Since $\log(\tilde{K})$ should be close to zero

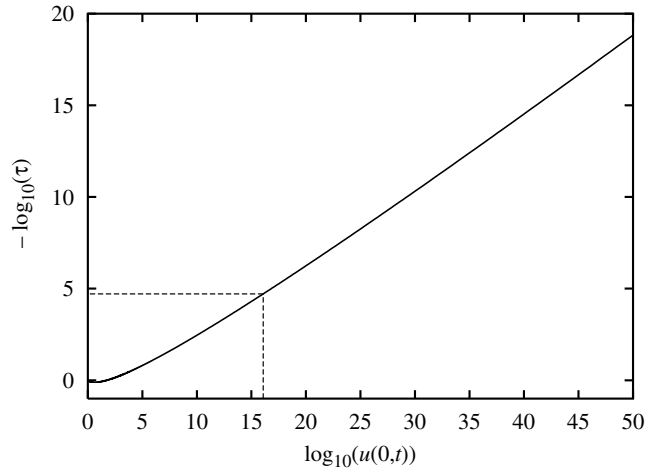

Fig. 13. The variation of $\log(\tau)$ as a function of $\log(u(0))$ to give a mesh which evolves smoothly.

and $\alpha \to 0$, it is reasonable to ignore the $\tilde{K}$ term. Using these relationships, $\log(\tau)$ as a function of $\log(u(0,t))$ is plotted in Fig. 13. Asymptotically, for large $u(0,t)$ we then have

$$-\log(\tau) \approx \frac{1}{2}\log(u) - \sqrt{2}\sqrt{\log(u)} + 1 + \mathcal{O}\left(1/\sqrt{\log(u)}\right).$$

For example, with $\beta = 1/2$ we can successfully integrate until $u(0,t) = 10^{16}$ provided that we take $\tau = 10^{-5}$ (see dashed lines in Fig. 13).

In the numerics presented in the previous sections, we used $\tau = 10^{-10}$ allowing a correct time scale for $u(0,t)$ up to $\approx 0^{30}$ – this is well beyond the typical break down of our numerics at $u(0,t) \approx 10^{21}$.

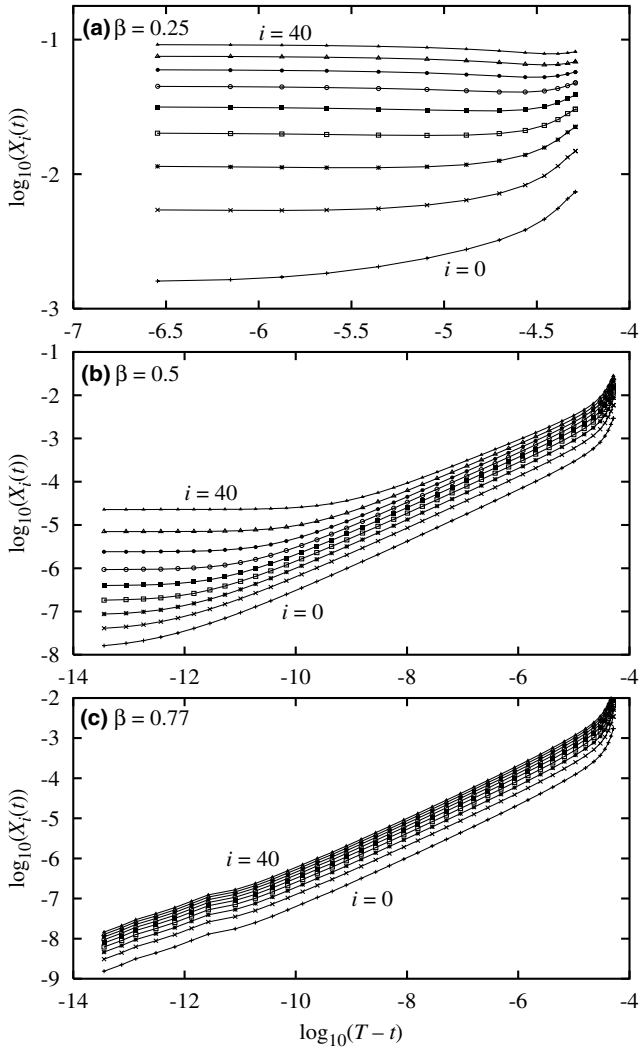

Fig. 14. Mesh points $X_i(t)$ evolution near blow-up time T for different monitor function exponents β. We depict the mesh points $X_i(t)$ for $i = 0,5,10,\ldots,40$.

5. Calculation of dynamic mesh location

To illustrate the results of the previous section, we solve the chemotaxis problem (1) using (15) with $\tau = 10^{-5}$ and $M(u) = u^{\beta}$ for $\beta = 0.25$, 0.5, and 0.77. In Fig. 14, we plot $\log(X_i)$ as a function of $\log(T - t)$ for these three cases.

For $\beta = 0.25$ the mesh evolves slowly, and early on it ceases evolving altogether, with the first mesh point placed at 10^{-3}. The natural length scale of the problem is given by $L(t) = (T - t)^{0.5 + \alpha} \approx (T - t)^{0.65}$. If $(T - t) \approx 10^{-6}$ all resolution is lost and *oscillations* in the computed solution occur due to an insufficient resolution of the peak (cf. Fig. 12). An example of the oscillations induced by the loss of resolution at the core is depicted in Fig. 15. Efforts are currently underway to analyse the mechanism behind these oscillations.

For $\beta = 0.5$ the mesh points evolve rapidly and stay close to the natural length scale until $(T - t) \approx 10^{-9}$. For smaller values of $(T - t)$ some mesh points cease to evolve, although those closest to the core region continue to evolve at the correct rate until $(T - t) \approx 10^{-13}$. We can compare this with the estimate of τ in (35) for the proper mesh evolution: If $\alpha = 0.15$, the mesh ceases to evolve for $\tau = 10^{-5}$ when $(T - t) \approx 10^{-14}$, which is more or less consistent with the above observations. At the final value of $(T - t)$ there is a very large variation between the smallest ($\sim 10^{-12}$) and the largest mesh spacings ($\sim 10^{-2}$).

As predicted, for $\beta = 0.77$ the mesh evolves very rapidly initially and then closely follows the natural length scale. However, the MMPDE calculation is very stiff, and features of the solution away from the singularity are not as well resolved.

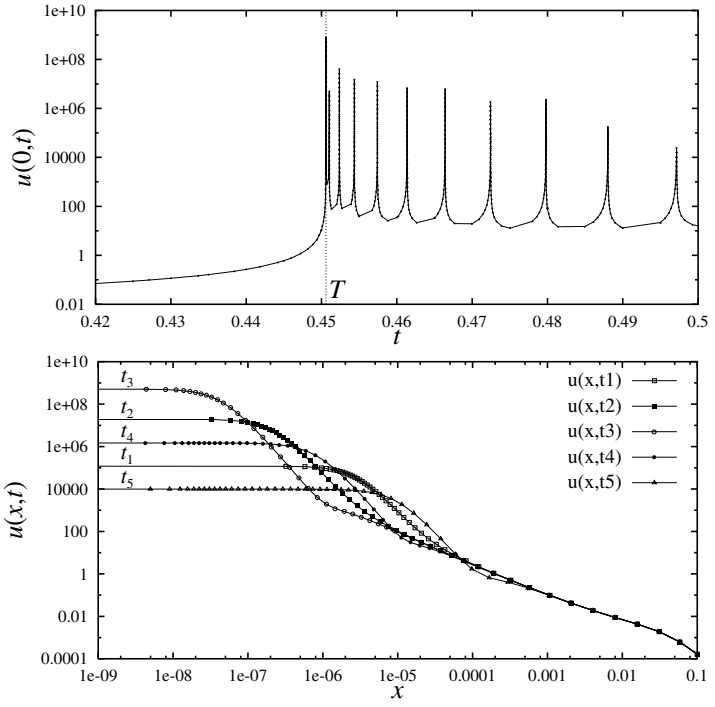

Fig. 15. Typical oscillations of the aggregate caused by loss of resolution at the core. The top panel displays maximum cell density $u(0,t)$ as a function of time. As time approaches T, cell density grows rapidly and then exhibits spurious oscillations. The bottom panel displays a series of snapshots for density profile just before blow-up ($t_1 < t_2 < T$), very close to blow-up time ($t_3 \approx T$), and just after blow-up ($T < t_4 < t_5$).

6. Conclusion

We have described an adaptive numerical method which can be designed to resolve difficulties associated with solutions of blow-up problems for reaction diffusion equations. The method can be used for general systems of PDEs, and for the chemotaxis problem considered here we solve the full system (1) directly.

In 2D, the radially symmetric solution to this problem, analysed in [2], is approximately self-similar, and capturing the fine details numerically requires very accurate computation of the solution very close to blow-up. There is considerable sensitivity inherent in this calculation, and in fact, in [1], facing numerical difficulties, the authors left this problem as one requiring further study. However, the method we develop in this paper appears ideally suited to reaction-diffusion equations of this type.

A key to the success of our MMPDE approach is the ability to build scale-invariance into the adaptive remeshing procedure. Even so, there are difficulties with the 2D problem, and careful analysis to determine a suitable monitor function is essential. Indeed, this problem illustrates the growing importance of the close interplay between analysis and computation necessary to resolve fine solution structure (in this case, characterised by the $\log(T-t)$ term in the asymptotic solution form).

It appears that this problem is also an important one physically, since chemotaxis can take place along surfaces or, e.g., air–water interfaces [17], and these have 2D problem features. Finally, we note that in the 3D problem there is also a set of stable non self-similar blow-up profiles which are *not* concentrated at the origin and have a ring like structure [23]. We are in the process of investigating these ring type solutions numerically [31].

Acknowledgements

CJB was funded through the EPSRC grant GR/T06377/01. RCG was partially supported by a grant from the SDSU Foundation. RDR acknowledges the support from NSERC (Canada) grant A8781. We are grateful to the anonymous reviewers for their careful review of this manuscript and their helpful comments and suggestions.

References

[1] M.D. Betterton, M.P. Brenner, Collapsing bacterial cylinders, Phys. Rev. E 64 (2001) 61904.
[2] M.A. Herrero, J.J.L. Velázquez, Singularity patterns in a chemotaxis model, Math. Ann. 306 (1996) 583–623.
[3] E.F. Keller, L.A. Segel, Initiation of slime mold aggregation viewed as an instability, J. Theo. Biol. 6 (1970) 399–415.
[4] E.F. Keller, L.A. Segel, Model for chemotaxis, J. Theo. Biol. 26 (1971) 225–234.
[5] E.F. Keller, L.A. Segel, Traveling bands of chemotactic bacteria: a theoretical analysis, J. Theo. Biol. 30 (1971) 235–248.
[6] M.P. Brenner, T.P. Witelski, On Spherically Symmetric Gravitational Collapse, preprint, 1998.
[7] P. Biler, T. Nadzieja, Global and exploding solutions in a model of self-gravitating systems, preprint.
[8] T. Hanawa, K. Nakayama, Stability of similarity solutions for a gravitationally contracting isothermal sphere: convergence to the Larson–Penston solution, The Astrophys. J. 484 (1997) 238–244.
[9] I.A. Guerra, Stabilization and Blow-up for some Multidimensional Nonlinear PDEs, PhD Thesis, TU Eindhoven, 2003.
[10] H.A. Levine, B.D. Sleeman, A system of reaction diffusion equations arising in the theory of reinforced random walks, SIAM J. Appl. Math. 57 (3) (1997) 683–730.
[11] J.J.L. Velázquez, Stability of some mechanisms of chemotactic aggregation, SIAM J. Appl. Math. 62 (5) (2002) 1581–1633.
[12] C.J. Budd, W. Huang, R.D. Russell, Moving mesh methods for problems with blow-up, SIAM J. Sci. Comput. 17 (2) (1996) 305–327.
[13] W. Huang, R.D. Russell, A moving collocation method for the numerical solution of time dependent partial differential equations, Appl. Numer. Math. 20 (1996) 101–116.
[14] W. Huang, Y. Ren, R.D. Russell, Moving mesh partial differential equations based on the equidistribution principle, SIAM J. Numer. Anal. 31 (1994) 709–730.

[15] W. Huang, Y. Ren, R.D. Russell, Moving mesh methods based on moving mesh partial differential equations, J. Comput. Phys. 113 (1994) 279–290.
[16] C.J. Budd, R.D. Russell, in preparation.
[17] H.G. Othmer, A. Stevens, Aggregation, blowup, and collapse: the ABC's of t-axis in reinforced random walks, SIAM J. Appl. Math. 57 (4) (1997) 1044–1081.
[18] W. Jäger, S. Luckhaus, On explosions of solutions to a system of partial differential equations modelling chemotaxis, Trans. Amer. Math. Soc. 329 (1992) 819–824.
[19] T. Nagai, Behavior of solutions to a parabolic-elliptic system modelling chemotaxis, J. Korean Math. Soc. 37 (2000) 721–733.
[20] T. Nagai, Blowup of nonradial solutions to parabolic-elliptic systems modelling chemotaxis in two-dimensional domains, J. Inequal. Appl. 6 (2001) 37–55.
[21] C.-S. Lin, W.-M. Ni, I. Takagi, Large amplitude stationary solutions to a chemotaxis system, J. Diff. Eq. 72 (1988) 1–27.
[22] W.-M. Ni, Diffusion, cross-diffusion, and their spike layer steady states, Notices Amer. Math. Soc. 45 (1998) 9–18.
[23] M.A. Herrero, E. Medina, J.J.L. Velázquez, Finite-time aggregation into a single point in a reaction-diffusion system, Nonlinearity 10 (1997) 1739–1754.
[24] M.A. Herrero, E. Medina, J.J.L. Velázquez, Self-similar blow-up for a reaction diffusion-system, J. Comput. Appl. Math. 97 (1998) 99–119.
[25] M.P. Brenner, P. Constantin, L.P. Kadanoff, A. Schenkel, S.C. Venkataramani, Diffusion, attraction and collapse, Nonlinearity 12 (1999) 1071–1098.
[26] L.R. Petzold, A description of DASSL: a differential/algebrasystem system solver, SAND 82-8637, Sandia Labs, Livermore, CA, 1982.
[27] J. Dongarra, J. Bunch, C. Moler, G.W. Stewart, Linpack Users' Guide, SIAM, Philadelphia, 1979.
[28] E. Hairer, G. Wanner, Solving Ordinary Differential Equations II: Stiff and Differential Algebraic ProblemsSpringer Series in Computational Mathematics, 14, Springer-Verlag, Berlin, 1996.
[29] S. Childress, J.K. Percus, Nonlinear aspects of chemotaxis, Math. Biosci. 56 (1981) 217–237.
[30] S. Childress, Chemotactic collapse in two dimensionsLecture Notes in Biomathematics, 55, Springer-Verlag, Berlin, 1984, pp. 61–66.
[31] C.J. Budd, R. Carretero-González, R.D. Russell. Blow-up rings in chemotactic collapse, in preparation.
[32] G. Beckett, J.A. Mackenzie, On a uniform accurate finite difference approximation of a singularly perturbed reaction-diffusion problem using grid equidistribution, J. Comput. Appl. Math. 131 (1–2) (2001) 381–405.